ATLAS NOTE

ATLAS-CONF-2016-022

12th May 2016

A search for R-parity violating decays of the top squark in four-jet final states with the ATLAS experiment at $\sqrt{s} = 13$ TeV

The ATLAS Collaboration

Abstract

We present a search for direct production of pairs of top squarks, each decaying into a b- and an s-quark through R-parity violating couplings. The analysis uses 3.2 fb^{-1} of proton-proton collision data recorded at $\sqrt{s}$=13 TeV by the ATLAS experiment at the LHC in 2015. Four jets, two of which are b-tagged, are selected and paired according to their angular separation. Signal regions are defined by imposing requirements on the masses of the two resonance candidates and their angular distribution. The average mass of the resonances is then used as the final discriminant. No significant excess is observed above the background prediction and a 95% confidence level lower limit on the mass of the top squark in the model considered of 345 GeV is derived.

ATLAS-CONF-2016-022
12 May 2016

1 Introduction

Massive coloured particles decaying into quarks are predicted in several extensions of the Standard Model (SM). At hadron colliders, the search for new phenomena in fully hadronic final states, without missing transverse energy or leptons, is experimentally challenging because of the very large multijet production cross-section. This note presents a search for the pair production of resonances each decaying into two SM quarks using 3.2 fb^{-1} of $\sqrt{s}$ = 13 TeV proton–proton (pp) collision data recorded by the ATLAS experiment at the Large Hadron Collider (LHC).

Supersymmetry (SUSY) [1–6] is a generalization of the Poincaré symmetry group that fundamentally relates fermionic and bosonic degrees of freedom. In the generic superpotential, Yukawa couplings can lead to baryon- and lepton-number violation:

$$\mathcal{W}_{\mathrm{RPV}} = \kappa_i L_i H_d + \lambda_{ijk} L_i L_j \bar{E}_k + \lambda'_{ijk} L_i \bar{Q}_j \bar{D}_k + \lambda''_{ijk} \bar{U}_i \bar{D}_j \bar{D}_k, \tag{1}$$

where i, j, k are generation indices. While these terms in many scenarios are removed by imposing an additional Z_2 symmetry (R-parity) [7], the possibility that at least some of these R-parity violating (RPV) couplings are not zero is not ruled out experimentally. This family of models leads to unique collider signatures which would elude conventional searches for R-parity conserving SUSY. Scenarios in which any of the λ'' couplings are not zero are often referred to as UDD scenarios.

This search specifically targets pair production of the top squark[1] (stop) which decays via the λ''_{323} coupling, thus resulting in the process $\tilde{t} \to \bar{b}\bar{s}$ (assuming a 100% branching ratio), depicted in Fig. 1. The aim of the analysis is to achieve sensitivity for stop production at high masses, taking advantage of the increase in the signal cross-section at $\sqrt{s}$ = 13 TeV. Naturalness arguments [8, 9] suggests higgsinos and stops to be light, with masses below a TeV [10, 11]. Third generation squarks in R-parity conserving scenarios, and stops in particular, have been the subject of a thorough programme of searches at the LHC [12–14]. Current indirect experimental constraints [15] on the sizes of each of the UDD couplings λ'' from sources other than proton decay are primarily valid for low squark mass and for first- and second-generation couplings. In theories with minimal flavour violation [16], in which the flavour and CP-violating interactions of SUSY particles are governed by the SM Cabibbo-Kobayashi-Maskawa matrix, only the λ''_{323} coupling is significant [17] resulting in prompt decays of the stop into $\tilde{t} \to \bar{b}\bar{s}$.

Previous searches for pair produced resonances in hadronic final states have been performed at 7 and 8 TeV by both the ATLAS [18, 19] and CMS experiments [20, 21]. For stop decays including heavy-flavour jets in the final state exclusion limits at 95% confidence level (CL) between $100 \leq m_{\tilde{t}} \leq 320$ GeV and $200 \leq m_{\tilde{t}} \leq 385$ GeV have been reported by ATLAS [19] and CMS [21], respectively. In addition two ATLAS searches [22, 23] have placed constraints on RPV stops that decay to bs when they are produced in the decays of light gluinos. Further searches targeting the production of gluinos decaying through UDD couplings have been performed by both the ATLAS [24] and CMS [25] collaborations.

This note is organised as follows: in Section 2 an overview the ATLAS detector is presented, Section 3 describes the data and simulated event samples. Section 4 discuss the definitions of the objects used in the analysis, and Section 5 the event selections. The background estimate is presented in Section 6 with the systematic uncertainties discussed in Section 7. Finally the results of the analysis and the statistical interpretation are given in Section 8.

[1] The superpartners of the left- and right-handed top quarks, $\tilde{t}_L$ and $\tilde{t}_R$, mix to form the two mass eigenstates $\tilde{t}_1$ and $\tilde{t}_2$, where $\tilde{t}_1$ is the lightest one. This analysis considers only the production of the $\tilde{t}_1$, which thereafter is simply refererred to as $\tilde{t}$.

2 ATLAS detector

The ATLAS detector [26] is a multi-purpose particle physics detector with a forward-backward symmetric cylindrical geometry and nearly 4π coverage in solid angle[2]. The inner tracking detector consists of pixel and silicon microstrip detectors covering the pseudorapidity region $|\eta| < 2.5$, surrounded by a transition radiation tracker which enhances electron identification in the region $|\eta| < 2.0$. Starting in Run-2, a new inner pixel layer, the Insertable B-Layer (IBL) [27], has been inserted at a mean sensor radius of 3.3 cm. The inner detector is surrounded by a thin superconducting solenoid providing an axial 2 T magnetic field and by a fine-granularity lead/liquid-argon (LAr) electromagnetic calorimeter covering $|\eta| < 3.2$. A steel/scintillator-tile calorimeter provides hadronic coverage in the central pseudorapidity range ($|\eta| < 1.7$). The endcap and forward regions ($1.5 < |\eta| < 4.9$) of the hadronic calorimeter are made of LAr active layers with either copper or tungsten as the absorber material. An extensive muon spectrometer with an air-core toroid magnet system surrounds the calorimeters. Three layers of high-precision tracking chambers provide coverage in the range $|\eta| < 2.7$, while dedicated fast chambers allow triggering in the region $|\eta| < 2.4$. The ATLAS trigger system consists of a hardware-based level-1 trigger followed by a software-based high level trigger [28].

3 Data and simulated event samples

The data used in this analysis were collected by the ATLAS detector in pp collisions at the LHC using a centre-of-mass energy of 13 TeV and a 25 ns minimum proton bunch crossing interval during 2015. Events were recorded using a four-jet trigger with transverse energy thresholds of 85 GeV at the high level trigger which is fully efficient after the analysis selections are applied. After requiring beam, data, and detector quality criteria, the available dataset corresponds to an integrated luminosity of 3.2 fb^{-1} with an associated uncertainty of ±5% derived from a preliminary calibration of the luminosity scale using a pair of x-y beam-separation scans performed in August 2015, following a methodology similar to that which is detailed in Ref. [29].

The dominant background of SM multijet production is estimated with a data-driven technique, while Monte Carlo (MC) simulated events are used to model the signals and to establish and validate the background estimation method. The small background contribution from top pair production is also estimated using MC simulation. Interactions with the detector are modeled using a GEANT4-based simulation [30, 31]. To account for additional pp interactions from the same and close-by bunch crossings (pileup), a set of minimum bias interactions is generated using PYTHIA 8.186 [32] with the A2 tune [33] and the MSTW2008LO [34, 35] parton density function (PDF) set and is superimposed on the hard scattering events. The EvtGen v1.2.0 program [36] is used to simulate properties of bottom and charm hadron decays for all samples.

[2] ATLAS uses a right-handed coordinate system with its origin at the nominal interaction point in the centre of the detector. The positive x-axis is defined by the direction from the interaction point to the centre of the LHC ring, with the positive y-axis pointing upwards, while the beam direction defines the z-axis. Cylindrical coordinates (r, ϕ) are used in the transverse plane, ϕ being the azimuthal angle around the z-axis. The pseudorapidity η is defined in terms of the polar angle θ by $\eta = -\ln\tan(\theta/2)$. Rapidity is defined as $y = 0.5 \cdot \ln[(E + p_z)/(E - p_z)]$ where E denotes the energy and p_z is the component of the momentum along the beam direction.

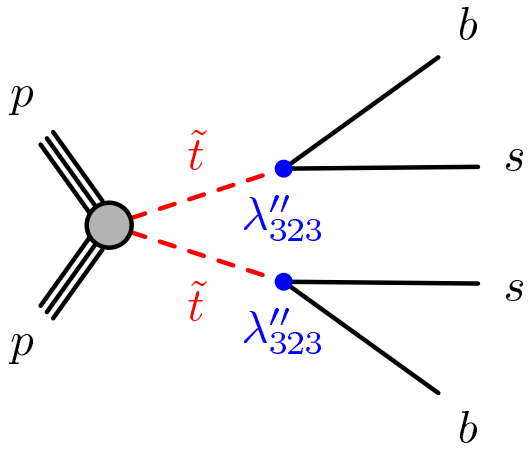

Figure 1: Direct production of stops, in red, decaying into a b- and an s-quark through the RPV λ'' coupling, indicated by the blue dots.

Background samples of multijet production are simulated with multiple $2 \to 2$ matrix elements (ME) at leading order (LO) using the Pythia 8.186 generator. The A14 tune [37] of shower and multiple parton interactions parameters is used together with the NNPDF23LO PDF set [38].

Top pair production events are simulated using the Powheg-Box v2 [39] generator with the CT10 [40] PDF set, as detailed in [41]. The top mass is set to 172.5 GeV. The h_{damp} parameter, which regulates the transverse momentum (p_{T}) of the first extra emission beyond the Born configuration and thus controls the p_{T} of the $t\bar{t}$ system, is set to the mass of the top quark. The parton shower (PS), fragmentation, and the underlying event are simulated using Pythia 6.428 [42] with the CTEQ6L1 [43] PDF set and the corresponding Perugia 2012 tune (P2012) [44]. The sample is normalized to the next-to-next-to-leading order cross-section including the resummation of soft gluon emission at next-to-next-to-logarithmic accuracy using `Top++2.0` [45].

The stop signal samples are generated using MG5_aMC@NLO [46] v2.2.3 interfaced to Pythia 8.186 with the A14 tune for the modeling of the parton showering, hadronization and underlying event. The ME calculation is performed at tree-level and includes the emission of up to two additional partons. The PDF set used for the generation is NNPDF23LO. The ME/PS matching is done using the CKKW-L [47] prescription, with a matching scale set to one quarter of the pair-produced stop mass. All non-SM particle masses are set to 5 TeV except for the stop mass ($m_{\tilde{t}}$), which is scanned in steps of 25 GeV from $m_{\tilde{t}} = 250$ GeV to $m_{\tilde{t}} = 650$ GeV. The two stops are then forced to decay promptly into a b- and an s-quark each. Signal cross-sections are calculated to next-to-leading order in the strong coupling constant, adding the resummation of soft gluon emission at next-to-leading-logarithmic accuracy [48–50]. The nominal cross-section and its uncertainty are taken from an envelope of cross-section predictions using different PDF sets and factorization and renormalization scales, as described in Ref. [51].

4 Object reconstruction

Each event is required to have a reconstructed primary vertex consistent in location with the beamspot envelope and with at least two associated tracks with $p_{\mathrm{T}} > 400$ MeV [52]. If more than one such vertex

is found, the vertex with the largest $\sum p_{\mathrm{T}}^2$ of the associated tracks is chosen.

Candidate jets are reconstructed from three-dimensional topological energy clusters [53] in the calorimeter using the anti-k_t jet algorithm [54] with a radius parameter of 0.4. Each topological cluster is calibrated to the electromagnetic scale response prior to jet reconstruction. The reconstructed jets are then calibrated to the particle level by the application of a jet energy scale (JES) derived from simulation and in situ corrections based on 8 TeV data [55, 56] and validated with early Run-2 data. The expected event average energy contribution from pileup clusters is subtracted using a factor dependent on the jet area [56].

Quality criteria are imposed to identify jets arising from non-collision sources or detector noise and any event containing such a jet is removed [57].

Jets containing b-hadrons (b-jets) are tagged by a multivariate algorithm (referred to as MV2c20) using information about the impact parameters of inner detector tracks associated to the jet, the presence of displaced secondary vertices, and the reconstructed flight paths of b- and c-hadrons inside the jet [58, 59]. A b-tagging working point with a 77% efficiency, as measured in a simulated sample of $t\bar{t}$ events, is chosen. The corresponding rejection factors against jets originating from c-quarks and from light-quarks or gluons are 4.5 and 130, respectively. Corrections derived from data control samples are applied to account for differences between data and simulation for the efficiency and mis-tag rate of the b-tagging algorithm.

5 Event Selection

As the stops are produced on mass-shell the final state consists of four jets forming two pairs each with invariant masses close to that of the stop. Only events with at least four reconstructed jets with $p_{\mathrm{T}} > 150$ GeV and $|\eta| < 2.4$ are retained in the analysis. For the stop mass range considered, a significant fraction of the stops will be produced with a large transverse momentum. As a result we expect the decay products to be close-by in ΔR. Taking advantage of this property, candidate resonances are constructed by pairing the four leading jets in the event. Two jet pairs are identified by minimizing the following quantity:

$$\Delta R_{\mathrm{min}} = \sum_{i=1,2} |\Delta R_i - 1.0| \tag{2}$$

where $\Delta R_i = \sqrt{(\Delta\eta_i)^2 + (\Delta\phi_i)^2}$ is the angular distance between the two jets for the i^{th} pair and the sum is over the two pairs of dijets. The offset of -1.0 has been chosen to maximize the signal efficiency for the stop masses of interest while minimizing the effects of soft jets from radiated gluons being recombined with their parent jets in multijet topologies. In order to reduce the multijet background, where the quality of this pairing is expected to be poor, the event is discarded if the best combination of the four leading jets has $\Delta R_{\mathrm{min}} > 1.6$.

Additional selections are applied to further enhance the signal fraction. These are based on four discriminating variables established from simulation studies and previous ATLAS searches [18, 19].

The absolute value of the cosine of the stop-pair production angle in the center-of-mass frame with respect to the beamline is $|\cos(\theta^*)|$. Background jets from multijet production are frequently originating from t-channel gluon exchange and are preferentially produced in the forward region, while jets originating from stop decays are instead expected to be more central.

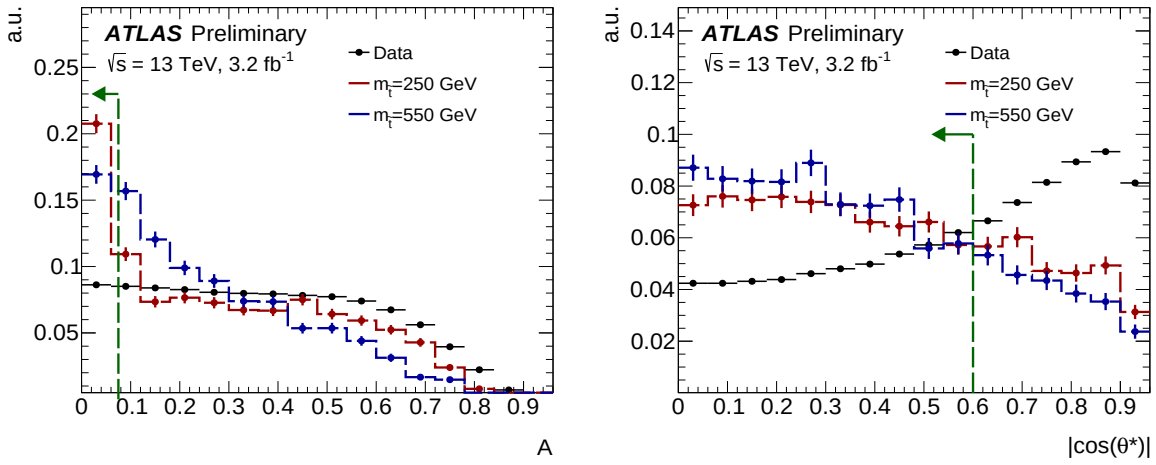

(a) (b)

Figure 2: Comparison of the shape of the $\mathcal{A}$ and $|\cos(\theta^*)|$ distributions for data and two signal point with $m_{\tilde{t}} = 250$ and 550 GeV. The distributions are normalised to unity and shown after the requirement of four jets paired into two candidate resonances. The green arrow indicates the requirement applied for the signal region selection.

Since the two reconstructed resonances are expected to have equal mass, their mass difference is a powerful discriminant between signal and background. The mass asymmetry ($\mathcal{A}$) is defined as:

$$\mathcal{A} = \frac{|m_1 - m_2|}{m_1 + m_2} \tag{3}$$

where m_1 and m_2 are the invariant masses of the two reconstructed dijet pairs. $\mathcal{A}$ is expected to be close to zero for well-paired signal events and is relatively flat for background events.

The distribution of $\mathcal{A}$ and $|\cos(\theta^*)|$ is shown for data and two signal samples with stop masses of $m_{\tilde{t}} = 250, 450$ GeV in Fig. 2(a) and 2(b) respectively. Given the very small amount of signal expected before additional selections are applied the data distribution can be viewed as representative of the background expectation. The signal region (SR) selection applies a requirement of of $\mathcal{A} < 0.075$ and $|\cos(\theta^*)| < 0.6$, following an optimization procedure maximizing the discovery significance.

Another quantity that is exploited for background discrimination is the number of b-tagged jets in the event. By requiring each of the reconstructed resonances to contain at least one b-tagged jet the multijet background can be significantly reduced.

The final analysis discriminant is the average mass of the two reconstructed resonances:

$$m_{\text{avg}} = \frac{1}{2}(m_1 + m_2)\,. \tag{4}$$

A peak in m_{avg} at a mass of about that of the stop is expected for the signal, over a non-peaking background from multijet processes. For each stop mass hypothesis a counting experiment is then performed in a window of the m_{avg} variable optimised to maximize the expected discovery significance. Fig. 3(a) shows the expected m_{avg} distribution for signal samples with different $m_{\tilde{t}}$ masses, while the acceptance times efficiency of the SR selections is shown before and after applying the m_{avg} mass window requirement in Fig. 3(b). The acceptance of the SR selection increases for large stop masses due to its decay products

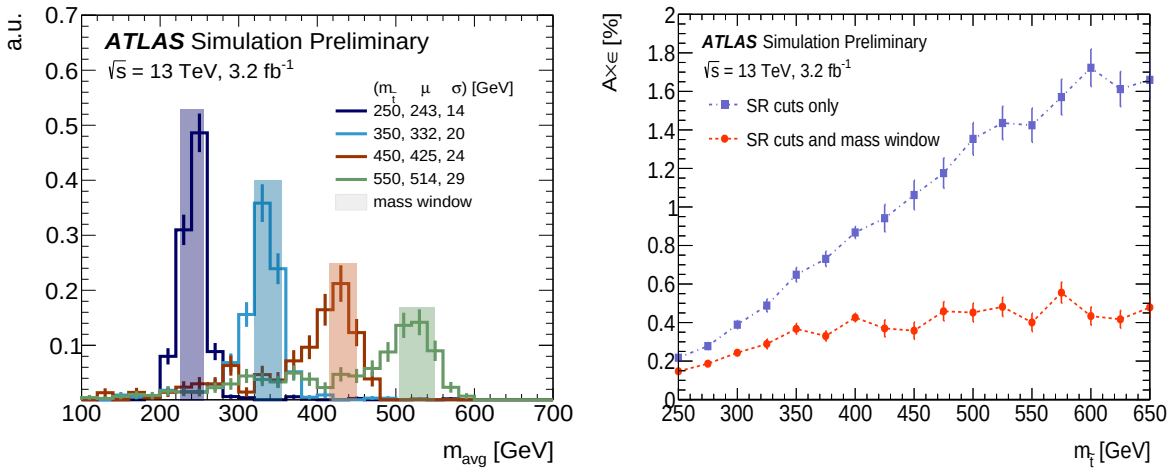

(a) (b)

Figure 3: 3(a): Distribution of the average mass m_{avg} for signal samples with $m_{\tilde{t}} = 250, 350, 450$ and 550 GeV (solid lines), with the mass windows used for the counting experiments highlighted by shaded rectangles. The mean and standard deviations obtained by gaussian fits to the signal peaks are quoted in the legend. 3(b): The acceptance times efficiency ($Acc. \times \epsilon$) of the SR selection is shown before and after the mass windows cuts are applied.

having larger p_{T}. However due to the jet pairing not properly assigning the stop decay products, at high mass the signal exhibits a tail extending to low m_{avg} values, degrading the efficiency of the mass window selection.

6 Background estimation

The dominant background of SM multijet production is estimated directly from data with a method that predicts both the normalization and the shape of the m_{avg} distribution. MC simulation is used to validate the method as well as to estimate the small contribution from top quark pair production[3]. The multijet background is estimated in two steps. The shape of the m_{avg} distribution is first predicted in a region with a b-tag veto (zero-tag) and then extrapolated to the signal region where at least two b-tagged jets, one associated to each dijet pair, are required (two-tag).

The m_{avg} spectrum in the zero-tag region is obtained from data with an ABCD method. The data sample is divided into one region where the signal selection is applied (D) and three background dominated control regions (A, B, and C). The variables used to define the different regions, summarised in Tab. 1, are $|\cos(\theta^*)|$ and $\mathcal{A}$. Provided the two variables defining the regions are uncorrelated, the amount of background in the region of interest D can be predicted from the observed number of events in the control regions as $N_D = N_B \times N_C / N_A$. This approach, which does not use data in region D, avoids potential contamination from signals of stop decays into light-flavor quarks. The correlation between the two variables has been tested in the multijet MC sample, where it amounts to less than 4%.

[3] In the mass region considered the top pair contributes less than 2% of the total background.

Table 1: Definition of the four regions used for data-driven background determination. Region D is the signal region.

Region	$\mathcal{A}$	$\lvert\cos(\theta^*)\rvert$
A	< 0.075	≥ 0.6
B	≥ 0.075	≥ 0.6
C	≥ 0.075	< 0.6
D	< 0.075	< 0.6

The ABCD prediction in the zero-tag region is validated with a closure test in a region where the selections of the signal region are applied, but with the asymmetry requirement changed to $0.075 < \mathcal{A} < 0.15$. The A, B and C regions for this validation region are defined analogously to the signal region by inverting the $\mathcal{A}$ and $|\cos(\theta^*)|$ requirements. The output of the ABCD prediction is found to be consistent with the observed data, and the difference is used to assign a systematic uncertainty, which varies from about two to ten percent as function of m_{avg}.

The zero-tag prediction obtained from the ABCD method is then extrapolated to the two b-tag plane by means of projection factors similarly to the approach described in [19]. The projection factors, in a given region X, are defined as the ratio between the number of events in the two- and zero-tag planes (N_{X2}/N_{X0}) after the top quark background is subtracted. Given that the mass windows considered in the search start at m_{avg}=225 GeV, all the projection factors are computed in the region m_{avg}>200 GeV, to avoid potential bias from the subtraction of the top pair production background. For the signal region prediction, the average of the projection factors P_{AC} from the signal-depleted regions A and C, where the signal region requirements are reverted one at a time, is used:

$$P_{AC} = \frac{1}{2}\left(\frac{N_{A2}}{N_{A0}} + \frac{N_{C2}}{N_{C0}}\right). \tag{5}$$

The projection factor from region B is not considered being farther away from the signal region. The underlying assumption of this method is that the m_{avg} shape for the background is invariant across b-tag multiplicities and that a single projection factor can be used for all regions of the $\mathcal{A}$,$|\cos(\theta^*)|$ plane. A validation of these assumptions has been performed in the MC for both the signal and control regions. The shape of m_{avg} in data (after subtracting the expected $t\bar{t}$ background) for various b-tag selections is shown in regions A and C in Fig. 4. It is found to be largely compatible across b-tag multiplicities, within large statistical uncertainties.

The signal contamination in regions A and C has been computed in the m_{avg}>200 GeV range for a signal with $m_{\tilde{t}} = 400$ GeV, and it amounts to 2.2% and 2.5%, respectively.

The validity of the data-driven method is also estimated directly in data by projecting the m_{avg} shape from the zero-tag plane in a validation region where exactly one b-tag is required, thus limiting the amount of signal contamination. Two additional validation regions with selections close to those of the signal region are defined to evaluate the quality of the background prediction in the two b-tag plane. The first region, VRa, requires $0 < |\cos(\theta^*)| < 0.6$ and $0.1 < \mathcal{A} < 0.25$; while the second, VRb, requires $0.6 < |\cos(\theta^*)| < 0.75$ and $0.0 < \mathcal{A} < 0.2$. In all of these regions a good agreement is observed between data and the data-driven background expectation over the full m_{avg} range considered.

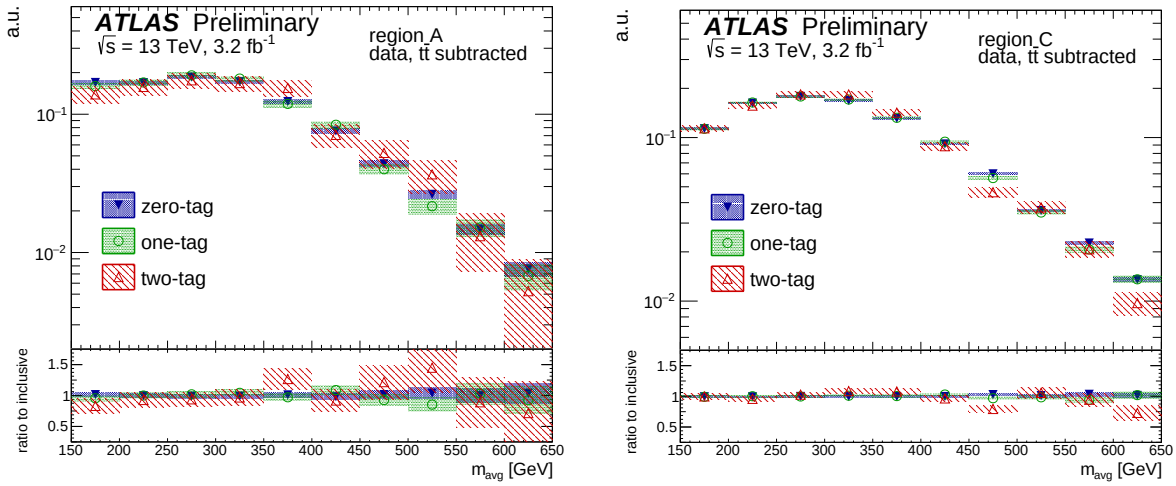

(a) region A

(b) region C

Figure 4: The m_{avg} spectrum in regions A and C in data for different b-tag multiplicities. The distributions are normalised to the integral of events with m_{avg}>150 GeV. The shaded and hatched bands include the statistical uncertainty of the samples.

7 Systematic uncertainties

Several sources of systematic uncertainty are considered when determining the estimated contributions from signal and background.

The multijet background uncertainties pertain primarily to the estimation method itself, as described in the previous section. The first systematic uncertainty considered is the non-closure uncertainty in the zero-tag plane. Additional systematic uncertainties are assigned to cover possible differences in the m_{avg} spectrum across b-tag multiplicities, the variations of the projection factors within the $\mathcal{A}$, $|\cos(\theta^*)|$ plane and differences in the jet calibrations for b- and light-jets. The projection factor is averaged over the A and C regions and the difference between the individual projection factors entering the average is assigned as an uncertainty to account for possible dependences within the $\mathcal{A}$, $|\cos(\theta^*)|$ plane. As the projection factor is assumed to be constant as function of m_{avg} an additional uncertainty is assigned by comparing it to the projection factors derived in 50 GeV wide bins of m_{avg}. The comparison is done separately in the A and C regions and the largest of the two differences is assigned as an uncertainty on the projection factor in each bin of m_{avg}. This uncertainty, which is the dominant one for this search, is largely dominated by the statistical uncertainty in the control regions. The different calibrations applied to b- and light-jets, could lead to differences in the m_{avg} shape across b-tag multiplicities. An uncertainty to account for this effect is assigned as a function of m_{avg} by computing the difference between the projection factors obtained with the nominal jet p_{T} selection varied from 150 to 140 or 160 GeV. The four sources of uncertainty are computed in 50 GeV bins in m_{avg}, which is close to the size of the mass windows used for the counting experiments, and further smoothed using a gaussian kernel with a 200 GeV bandwidth. The smoothed uncertainties are shown in Fig. 5 as a function of m_{avg}.

The estimated signal and top pair production yields, taken from MC, are effected by uncertainties related to the description of the detector response and the modelling of the physics process. The dominant

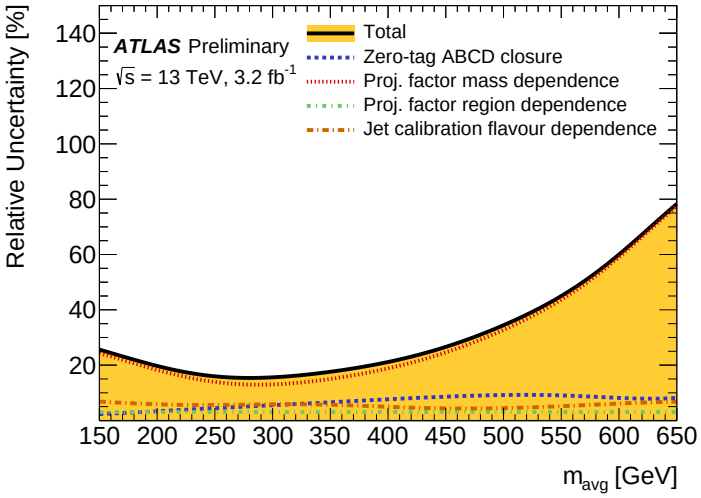

Figure 5: Systematic uncertainty for the data-driven multijet background estimation. The blue line shows the non-closure uncertainty in the zero-tag plane. The uncertainty due to the compatibility between the projection factors obtained in regions A and C is shown in green, while the uncertainty due to the jet measurement uncertainties is shown in brown. The dominant uncertainty, due to the m_{avg} dependence of the projection factors, is indicated by a red line.

detector-related systematic effects are due to the uncertainties on the jet energy scale (JES) [56] and resolution (JER) [55] and on the b-tagging efficiency and mistagging rates, estimated from 8 TeV data.

Systematic uncertainties related to the physics modelling of top pair production events are included. The systematic uncertainty related to the modeling of top pair production is taken as the difference between the predictions of the nominal sample and a alternative sample generated with MG5_aMC@NLO and showered with Herwig++ 2.7.1 [60]. This uncertainty amounts to 10% to 20% of the total expected top background in the m_{avg} range considered in the analysis and has a negligible impact on the results.

For the SUSY signal processes, both detector and theoretical uncertainties are considered. Each signal model is varied according to these systematic uncertainties and the impact on the acceptance and efficiency in each mass window is then propagated to the final result. The JES-related uncertainty on the predicted signal yield is up to 10% while the flavour-tagging uncertainties go up to 15% in specific mass windows

The nominal signal cross-sections and their uncertainties are taken from an envelope of cross-section predictions derived using different PDF sets and different factorization and renormalization scales, as described in Ref. [51]. The theoretical uncertainties on the acceptance of the signal simulation include variations of the renormalization and factorization scales, the CKKW-L merging scales, and the value of α_S in MG5_aMC@NLO as well as shower uncertainties in Pythia 8 evaluated from the A14 tune variations. The uncertainties are evaluated on a single signal point with $m_{\tilde{t}}$=250 GeV, as at low mass the effect of additional radiation becomes more important, and are assumed to be constant as function of $m_{\tilde{t}}$. After normalizing the samples to the same cross-section, the difference in the yield in the mass window, which is typically below 1%, is considered as an uncertainty.

8 Results and interpretation

The m_{avg} distribution in the two-tag signal region selection is shown in Fig. 6. The data are compared with the prediction obtained by projecting the background from the zero-tag plane. The observed number of events in each mass window, with the total background prediction and the expected signal yield is shown in Tab. 2. The contribution from top quark pair production amounts to less than 2% in any of the mass windows considered. The compatibility of the observed number of events with the background-only hypothesis is quantified in each mass window using p_0-values.

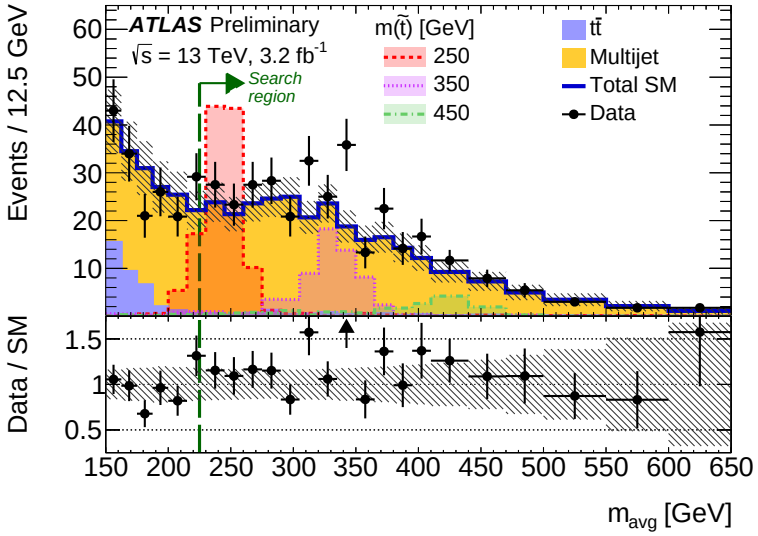

Figure 6: The observed m_{avg} spectrum in the signal region (black points) compared to the total background prediction (blue line). Also shown are the separate contributions of the multijet background, estimated with the projection method, and the $t\bar{t}$ obtained from simulation. All systematic uncertainties on the background estimate are included in the grey hatched band. The expected signal distributions for a few representative signal points are overlaid.

In the absence of a statistically significant excess in data, exclusion limits can be derived on the signal models of interest. A profile likelihood ratio combining Poisson probabilities for signal and background is computed to determine the 95% CL for compatibility of the data with the signal-plus-background hypothesis (CL_{s+b}) [61]. A similar calculation is performed for the background-only hypothesis (CL_b). From the ratio of these two quantities, the confidence level for the presence of a signal (CL_s) is determined [62]. Systematic uncertainties are treated as nuisance parameters and are assumed to follow Gaussian distributions. This procedure is implemented using a software framework for statistical data analysis, HistFitter [63]. The observed and expected 95% CL upper limits on the allowed cross-section are shown in Fig. 7. For stop decays into bs, the expected limit excludes stop masses up to 410 GeV, while the observed mass limit goes up to 345 GeV, improving on the previous ATLAS limit of 320 GeV[4].

[4] Due to a change in the convention for reporting observed limits, where the nominal signal cross-section is now considered, the value reported here is different from what quoted in [19].

$m(\tilde{t})$ [GeV]	Window [GeV]	Signal (± stat. ± sys.)	Expected background (± stat. ± sys.)	Data	p_0
250	[225 - 255]	102 ± 6 ± 12	53.8 ± 2.5 ± 8.7	68	0.10
275	[250 - 280]	80 ± 6 ± 11	54.6 ± 2.5 ± 8.2	62	0.25
300	[275 - 305]	66 ± 4 ± 8	59.5 ± 2.7 ± 8.9	59	0.50
325	[295 - 330]	52 ± 5 ± 7	61.0 ± 2.7 ± 9.5	73	0.19
350	[320 - 355]	44.6 ± 3.4 ± 7.2	57.7 ± 2.6 ± 9.5	80	0.07
375	[345 - 375]	27.7 ± 2.2 ± 3.7	39.7 ± 2.0 ± 7.0	48	0.27
400	[365 - 400]	25.1 ± 1.3 ± 3.6	41.8 ± 2.1 ± 8.0	52	0.25
425	[390 - 425]	15.6 ± 1.9 ± 1.8	31.9 ± 1.7 ± 6.8	40	0.23
450	[415 - 450]	10.9 ± 1.3 ± 1.5	24.3 ± 1.4 ± 5.8	30	0.27
475	[435 - 475]	10.3 ± 1.1 ± 1.3	23.5 ± 1.4 ± 6.2	23	0.50
500	[460 - 500]	7.5 ± 0.8 ± 1.4	18.1 ± 1.2 ± 5.5	20	0.45
525	[485 - 525]	6.0 ± 0.6 ± 0.9	13.7 ± 1.0 ± 4.7	7	0.50
550	[505 - 550]	3.8 ± 0.4 ± 0.7	9.9 ± 0.9 ± 3.9	9	0.50
575	[530 - 575]	4.0 ± 0.4 ± 0.8	8.3 ± 0.8 ± 3.7	13	0.28
600	[555 - 600]	2.42 ± 0.26 ± 0.46	7.3 ± 0.8 ± 3.8	5	0.50
625	[580 - 625]	1.82 ± 0.20 ± 0.28	5.7 ± 0.7 ± 3.4	5	0.50
650	[600 - 650]	1.64 ± 0.17 ± 0.34	4.4 ± 0.6 ± 3.0	7	0.25

Table 2: The observed number of data events and the total background prediction for each signal mass window of the signal region selection. The expected number of signal events is also shown. The significance of an excess can be quantified by the probability (p_0) that a background-only experiment is more signal-like than observed, bounded above by 0.5.

9 Conclusion

A search has been presented for the pair production of stops decaying into a b- and an s-quark. Four jets are reconstructed and paired into two candidate resonances according to their angular separation. Further selections based on their angular distributions and difference in mass are applied to enhance the fraction of signal. The average mass of the two candidate stops is used as final discriminant to define signal regions. The results are interpreted in a SUSY model with pair production of stop quarks decaying into two jets through the λ'' R-parity violating coupling. For decays into a b- and an s-quark, masses of the stop from 250 to 345 GeV are excluded at 95% CL, extending the previous ATLAS limit.

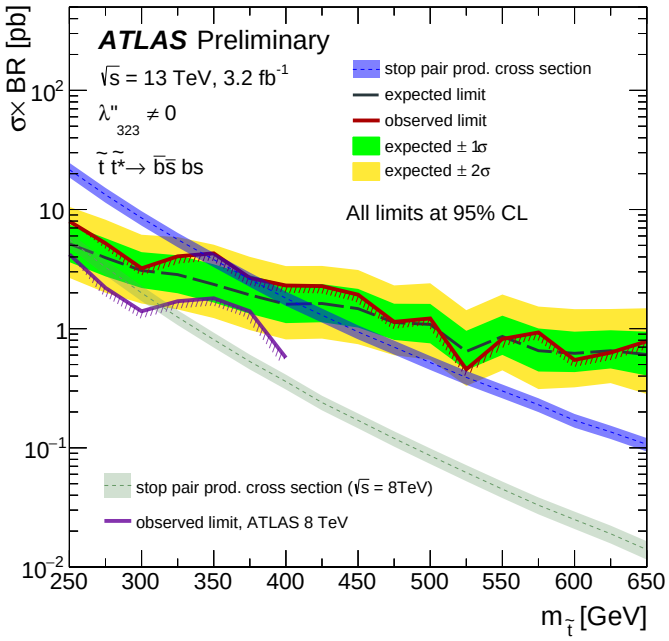

Figure 7: Expected and observed 95% CL upper limit on the $\sigma \times BR$ for the signal regions, compared to the theoretical cross-section for direct stop production with decays to a pair of jets. The dashed black and solid red lines show the 95% CL expected and observed limits respectively. The solid green (yellow) band around the expected limit show the one (two) sigma uncertainties around this limit. The dashed blue line indicates the nominal signal production cross-section with the shaded bands representing the $\pm 1\sigma$ variations due to theoretical uncertainties given by renormalization and factorization scale and PDF uncertainties. The observed exclusion limit from the 8 TeV ATLAS search [19] is also superimposed.

References

[1] Yu. A. Golfand and E. P. Likhtman,
Extension of the Algebra of Poincare Group Generators and Violation of p Invariance,
JETP Lett. **13** (1971) 323, [Pisma Zh. Eksp. Teor. Fiz.13,452(1971)].

[2] D. V. Volkov and V. P. Akulov, *Is the Neutrino a Goldstone Particle?*, Phys. Lett. **B46** (1973) 109.

[3] J. Wess and B. Zumino, *Supergauge Transformations in Four-Dimensions*,
Nucl. Phys. **B70** (1974) 39.

[4] J. Wess and B. Zumino, *Supergauge Invariant Extension of Quantum Electrodynamics*,
Nucl. Phys. **B78** (1974) 1.

[5] S. Ferrara and B. Zumino, *Supergauge Invariant Yang-Mills Theories*,
Nucl. Phys. **B79** (1974) 413.

[6] A. Salam and J. A. Strathdee, *Supersymmetry and Nonabelian Gauges*,
Phys. Lett. **B51** (1974) 353.

[7] G. R. Farrar and P. Fayet, *Phenomenology of the Production, Decay, and Detection of New Hadronic States Associated with Supersymmetry*, Phys. Lett. B **76** (1978) 575.

[8] R. Barbieri and G. F. Giudice, *Upper Bounds on Supersymmetric Particle Masses*,
Nucl. Phys. **B306** (1988) 63.

[9] B. de Carlos and J. A. Casas, *One loop analysis of the electroweak breaking in supersymmetric models and the fine tuning problem*, Phys. Lett. **B309** (1993) 320, arXiv: hep-ph/9303291.

[10] K. Inoue et al., *Aspects of Grand Unified Models with Softly Broken Supersymmetry*,
Prog. Theor. Phys. **68** (1982) 927, [Erratum: Prog. Theor. Phys.70,330(1983)].

[11] J. R. Ellis and S. Rudaz, *Search for Supersymmetry in Toponium Decays*,
Phys. Lett. **B128** (1983) 248.

[12] ATLAS Collaboration, *ATLAS Run 1 searches for direct pair production of third-generation squarks at the Large Hadron Collider*, Eur. Phys. J. C **75** (2015) 510,
arXiv: hep-ex/1506.08616.

[13] CMS Collaboration, *Search for direct pair production of scalar top quarks in the single- and dilepton channels in proton-proton collisions at* $\sqrt{s} = 8$ *TeV*, (2016),
arXiv: hep-ex/1602.03169.

[14] CMS Collaboration, *Search for direct pair production of supersymmetric top quarks decaying to all-hadronic final states in pp collisions at* $\sqrt{s} = 8$ *TeV*, (2016), arXiv: hep-ex/1603.00765.

[15] B. C. Allanach, A. Dedes and H. K. Dreiner,
Bounds on R-parity violating couplings at the weak scale and at the GUT scale,
Phys. Rev. **D60** (1999) 075014, arXiv: hep-ph/9906209.

[16] G. D'Ambrosio et al., *Minimal flavor violation: An Effective field theory approach*,
Nucl. Phys. **B645** (2002) 155, arXiv: hep-ph/0207036.

[17] C. Csaki, Y. Grossman and B. Heidenreich, *MFV SUSY: A Natural Theory for R-Parity Violation*,
Phys. Rev. **D85** (2012) 095009, arXiv: hep-ph/1111.1239.

[18] ATLAS Collaboration, *Search for pair-produced massive coloured scalars in four-jet final states with the ATLAS detector in proton–proton collisions at* $\sqrt{s} = 7$ *TeV*,
Eur. Phys. J. C **73** (2013) 2263, arXiv: hep-ex/1210.4826.

[19] ATLAS Collaboration, *A search for top squarks with R-parity-violating decays to all-hadronic final states with the ATLAS detector in* $\sqrt{s} = 8$ *TeV proton–proton collisions*, (2016), arXiv: hep-ex/1601.07453.

[20] CMS Collaboration, *Search for pair-produced dijet resonances in four-jet final states in pp collisions at* $\sqrt{s} = 7$ *TeV*, Phys. Rev. Lett. **110** (2013) 141802, arXiv: hep-ex/1302.0531.

[21] CMS Collaboration, *Search for pair-produced resonances decaying to jet pairs in proton–proton collisions at* $\sqrt{s} = 8$ *TeV*, Phys. Lett. B **747** (2015) 98, arXiv: hep-ex/1412.7706.

[22] ATLAS Collaboration, *Search for new phenomena in final states with large jet multiplicities and missing transverse momentum at* $\sqrt{s} = 8$ *TeV proton–proton collisions using the ATLAS experiment*, JHEP **1310** (2013) 130, arXiv: hep-ex/1308.1841.

[23] ATLAS Collaboration, *Search for supersymmetry at* $\sqrt{s} = 8$ *TeV in final states with jets and two same-sign leptons or three leptons with the ATLAS detector*, JHEP **1406** (2014) 035, arXiv: hep-ex/1404.2500.

[24] ATLAS Collaboration, *Search for massive supersymmetric particles decaying to many jets using the ATLAS detector in pp collisions at* $\sqrt{s} = 8$ *TeV*, Phys. Rev. D **91** (2015) 112016, arXiv: hep-ex/1502.05686.

[25] CMS Collaboration, *Searches for light- and heavy-flavour three-jet resonances in pp collisions at* $\sqrt{s} = 8$ *TeV*, Phys. Lett. B **730** (2014) 193, arXiv: hep-ex/1311.1799.

[26] ATLAS Collaboration, *The ATLAS Experiment at the CERN Large Hadron Collider*, JINST **3** (2008) S08003.

[27] ATLAS Collaboration, *ATLAS Insertable B-Layer Technical Design Report*, (2010), URL: http://cds.cern.ch/record/1291633.

[28] ATLAS Collaboration, *2015 start-up trigger menu and initial performance assessment of the ATLAS trigger using Run-2 data*, ATL-DAQ-PUB-2016-001, 2016, URL: http://cds.cern.ch/record/2136007.

[29] ATLAS Collaboration, *Improved luminosity determination in pp collisions at* $\sqrt{s} = 7$ *TeV using the ATLAS detector at the LHC*, Eur. Phys. J. C **73** (2013) 2518, arXiv: hep-ex/1302.4393.

[30] ATLAS Collaboration, *The ATLAS Simulation Infrastructure*, Eur. Phys. J. C **70** (2010) 823, arXiv: hep-ex/1005.4568.

[31] S. Agostinelli et al., *GEANT4: A Simulation toolkit*, Nucl. Instrum. Meth. **A506** (2003) 250.

[32] T. Sjöstrand, S. Mrenna and P. Z. Skands, *A Brief Introduction to PYTHIA 8.1*, Comput. Phys. Commun. **178** (2008) 852, arXiv: hep-ph/0710.3820.

[33] ATLAS Collaboration, *Summary of ATLAS Pythia 8 tunes*, ATL-PHYS-PUB-2012-003, 2012, URL: http://cds.cern.ch/record/1474107.

[34] A. D. Martin et al., *Parton distributions for the LHC*, Eur. Phys. J. **C63** (2009) 189, arXiv: hep-ph/0901.0002.

[35] A. Sherstnev and R. S. Thorne, *Parton Distributions for LO Generators*, Eur. Phys. J. **C55** (2008) 553, arXiv: hep-ph/0711.2473.

[36] D. J. Lange, *The EvtGen particle decay simulation package*, Nucl. Instrum. Meth. **A462** (2001) 152.

[37] ATLAS Collaboration, *ATLAS Pythia 8 tunes to 7 TeV data*, ATL-PHYS-PUB-2014-021, 2014, URL: http://cdsweb.cern.ch/record/1966419.

[38] R. D. Ball et al., *Parton distributions with LHC data*, Nucl. Phys. **B867** (2013) 244, arXiv: hep-ph/1207.1303.

[39] S. Alioli et al., *A general framework for implementing NLO calculations in shower Monte Carlo programs: the POWHEG BOX*, JHEP **06** (2010) 043, arXiv: hep-ph/1002.2581.

[40] H.-L. Lai et al., *New parton distributions for collider physics*, Phys. Rev. **D82** (2010) 074024, arXiv: hep-ph/1007.2241.

[41] ATLAS Collaboration, *Performance of primary vertex reconstruction in proton–proton collisions at* $\sqrt{s} = 7$ *TeV in the ATLAS experiment*, ATLAS-CONF-2010-069, 2010, URL: http://cdsweb.cern.ch/record/1281344.

[42] T. Sjostrand, S. Mrenna and P. Z. Skands, *PYTHIA 6.4 Physics and Manual*, JHEP **05** (2006) 026, arXiv: hep-ph/0603175.

[43] D. Stump et al., *Inclusive jet production, parton distributions, and the search for new physics*, JHEP **10** (2003) 046, arXiv: hep-ph/0303013.

[44] P. Z. Skands, *Tuning Monte Carlo Generators: The Perugia Tunes*, Phys. Rev. **D82** (2010) 074018, arXiv: hep-ph/1005.3457.

[45] M. Czakon and A. Mitov, *Top++: A Program for the Calculation of the Top-Pair Cross-Section at Hadron Colliders*, Comput. Phys. Commun. **185** (2014) 2930, arXiv: hep-ph/1112.5675.

[46] J. Alwall et al., *The automated computation of tree-level and next-to-leading order differential cross sections, and their matching to parton shower simulations*, JHEP **07** (2014) 079, arXiv: hep-ph/1405.0301.

[47] L. Lonnblad and S. Prestel, *Matching Tree-Level Matrix Elements with Interleaved Showers*, JHEP **03** (2012) 019, arXiv: hep-ph/1109.4829.

[48] W. Beenakker et al., *Stop production at hadron colliders*, Nucl. Phys. **B515** (1998) 3, arXiv: hep-ph/9710451.

[49] W. Beenakker et al., *Supersymmetric top and bottom squark production at hadron colliders*, JHEP. **1008** (2010) 098, arXiv: hep-ph/1006.4771.

[50] W. Beenakker et al., *Squark and gluino hadroproduction*, Int.J.Mod.Phys. **A26** (2011) 2637, arXiv: hep-ph/1105.1110.

[51] M. Kramer et al., *Supersymmetry production cross sections in pp collisions at* $\sqrt{s} = 7$ *TeV*, (2012), arXiv: hep-ph/1206.2892.

[52] ATLAS Collaboration, *Vertex Reconstruction Performance of the ATLAS Detector at* $\sqrt{s} = 13$ *TeV*, ATL-PHYS-PUB-2015-026, 2015, URL: http://cdsweb.cern.ch/record/2037717.

[53] ATLAS Collaboration, *Topological cell clustering in the ATLAS calorimeters and its performance in LHC Run 1*, (2016), arXiv: hep-ex/1603.02934.

[54] M. Cacciari, G. P. Salam and G. Soyez, *The Anti-k(t) jet clustering algorithm*, JHEP **04** (2008) 063, arXiv: hep-ph/0802.1189.

[55] ATLAS Collaboration, *Monte Carlo Calibration and Combination of In-situ Measurements of Jet Energy Scale, Jet Energy Resolution and Jet Mass in ATLAS*, ATLAS-CONF-2015-037, 2015, URL: http://cdsweb.cern.ch/record/2044941.

[56] ATLAS Collaboration, *Jet Calibration and Systematic Uncertainties for Jets Reconstructed in the ATLAS Detector at* $\sqrt{s} = 13$ *TeV*, ATL-PHYS-PUB-2015-015, 2015, URL: http://cds.cern.ch/record/2037613.

[57] ATLAS Collaboration, *Selection of jets produced in* 13 *TeV proton–proton collisions with the ATLAS detector*, ATLAS-CONF-2015-029, 2015, URL: http://cdsweb.cern.ch/record/2037702.

[58] ATLAS Collaboration, *Commissioning of the ATLAS b-tagging algorithms using* $t\bar{t}$ *events in early Run 2 data*, ATL-PHYS-PUB-2015-039, 2015, URL: http://cdsweb.cern.ch/record/2047871.

[59] ATLAS Collaboration, *Performance of b-Jet Identification in the ATLAS Experiment*, (2015), arXiv: hep-ex/1512.01094.

[60] M. Bahr et al., *Herwig++ Physics and Manual*, Eur. Phys. J. **C58** (2008) 639, arXiv: hep-ph/0803.0883.

[61] G. Cowan et al., *Asymptotic formulae for likelihood-based tests of new physics*, Eur. Phys. J. **C71** (2011) 1554, [Erratum: Eur. Phys. J.C73,2501(2013)], arXiv: physics.data-an/1007.1727.

[62] A. L. Read, *Presentation of search results: The CL(s) technique*, J. Phys. **G28** (2002) 2693.

[63] M. Baak et al., *HistFitter software framework for statistical data analysis*, Eur. Phys. J. **C75** (2015) 153, arXiv: hep-ex/1410.1280.